EARTHQUAKE ENGINEERING AND STRUCTURAL DYNAMICS, VOL. 27, 109–124 (1998)

FLUID–STRUCTURE INTERACTION ANALYSIS OF 3-D RECTANGULAR TANKS BY A VARIATIONALLY COUPLED BEM–FEM AND COMPARISON WITH TEST RESULTS

HYUN MOO KOH*†, JAE KWAN KIM‡ AND JANG-HO PARK§
Department of Civil Engineering, Seoul National University, Seoul, Korea

SUMMARY

A variationally coupled BEM–FEM is developed which can be used to analyse dynamic response, including free-surface sloshing motion, of 3-D rectangular liquid storage tanks subjected to horizontal ground excitation. The tank structure is modelled by the finite element method and the fluid region by the indirect boundary element method. By minimizing a single Lagrange function defined for the entire system, the governing equation with symmetric coefficient matrices is obtained. To verify the newly developed method, the analysis results are compared with the shaking-table test data of a 3-D rectangular tank model and with the solutions by the direct BEM–FEM. Analytical studies are conducted on the dynamic behaviour of 3-D rectangular tanks using the method developed. In particular, the characteristics of the sloshing response, the effect of the rigidity of adjacent walls on the dynamic response of the tanks and the orthogonal effects are investigated. © 1998 John Wiley & Sons, Ltd.

Earthquake Engng. Struct. Dyn., **27**, 109–124 (1998)

KEY WORDS: fluid–structure interaction; rectangular tank; sloshing; indirect BEM–FEM

INTRODUCTION

The seismic response of liquid storage tanks can be strongly influenced by the interaction between the flexible containing structure and the contained fluid. The dynamic response of flexible liquid storage tanks may have characteristics significantly different from those of corresponding rigid storage tanks (for recent reviews on this subject see Reference 1), and has been studied extensively especially in connection with the seismic design of cylindrical tanks.[2–10]

Studies on the seismic response of rectangular tanks are quite rare,[11–14] while those concerning cylindrical tanks are abundant. Moreover in most existing studies on the rectangular tanks, the structure is assumed to be rigid.[11–13] Recently, Kim *et al.*[15] studied dynamic behaviour of 3-D rectangular flexible fluid containers using the Rayleigh–Ritz method. Their method is convenient and simple to use for practical purposes. However, in their study, only a pair of walls, orthogonal to the direction of the applied ground motion is assumed to be flexible while the other pair remain rigid and the effects of sloshing or surface waves are not taken into account.

* Correspondence to: Hyun M. Koh, Visiting Scholar, UC Berkeley, EERC, 1301 South 46th Street, Bldg. 451, Richmond, CA 94804-4698, U.S.A. E-mail: kohhyun@ce.berkeley.edu or kohhyun@gong.snu.ac.kr
† Professor
‡ Assistant Professor
§ Former doctoral graduate student, currently at DAEWOO Construction and Engineering Company

Contract grant sponsor: EESRI
Contract grant sponsor: KEPCO

CCC 0098–8847/98/020109–16$17·50

Received 20 June 1996
Revised 10 June 1997

Studies on the fluid–structure interaction in a domain of a more general geometry, other than the cylindrical shape, can be found in the literature on the seismic design of concrete gravity dams[16–20] or arch dams.[21–24] A dam–reservoir structure is a liquid storage structure of large scale. For such a system, it is necessary to take into account the fluid–structure (i.e. dam–reservoir) interaction effects. Even though the seismic design of dams and that of liquid storage tanks both involve fluid–structure interaction, the dam problem differs from the tank problem in the following points: in the dam problem, the associated fluid domain is very large and, consequently, is usually modelled as a semi-infinite region, while the tank problem deals with a finite fluid region of relatively small volume; the compressibility of the fluid is known to have significant effects on the dynamic response of dams, however, it is not the case in most tank problems; and the surface wave effects are usually neglected in the dynamic analysis of dams; on the other hand, the sloshing response is an important consideration in the seismic analysis of storage tanks, especially for storage tanks of nuclear spent fuel assemblies.

Dynamic analyses of gravity dams are performed using either 2-D[16–20] or 3-D[25,26] models. However, the use of 3-D models is unavoidable for the analysis of arch dams. Because of complexity in the analysis model, various substructure methods are preferred for the seismic analysis of dams.[16–19,21,23,24,26,27]. The coupled BEM–FEM[28–30] also has been successfully applied to dam problems. This hybrid approach is very attractive since a detailed description of the behaviour of the structure can be accomplished by finite element modelling while the motion of the homogeneous fluid region can be described with a very small number of degrees of freedom by boundary element modelling.

In this paper, a variationally coupled BEM–FEM is developed for the seismic response analysis of 3-D rectangular liquid storage tanks subjected to horizontal earthquake ground motion. Following verification, it is applied to study seismic response characteristics of 3-D rectangular tank models. Not only the interaction between the flexible structure and the stored liquid but also the effects of free-surface sloshing are taken into account within the limits of linearized boundary conditions.

In the proposed coupled BEM–FEM, the motion of a tank structure is modelled by the finite element method and the irrotational motion of the contained fluid region, which is assumed to be inviscid and comprised by an incompressible ideal fluid, by the boundary element method. A direct formulation has been adopted in many applications of BEM to the dam–reservoir problem. However, such a formulation may render the coefficient matrices of the equation asymmetric. Therefore, an indirect approach is taken in the present application of the BEM. This is because if the indirect BEM is used in connection with a variational principle, then the matrices in the governing algebraic equations will have symmetric forms. In the present method, the governing algebraic equations are derived by minimizing a single Lagrange function defined for the combined fluid–structure system. This particular variational formulation is essentially due to Luke[31] and Haroun[32] and is appropriate to model the fluid–structure interaction problems with the free liquid surface.

To verify the developed method, shaking-table experimental data of a small-scale 3-D rectangular acrylic tank are compared with the solutions obtained by the method proposed. The accuracy of the proposed method is examined further by comparing selected analysis results with those obtained using the direct BEM.

Characteristics of the dynamic behaviour of 3-D rectangular tanks are studied by the proposed method. Since a preliminary study on the dynamics of a 3-D rectangular tank already has been presented in our previous report,[15] emphasis will be placed mostly on the sloshing response, the effect of the flexibility of adjacent walls parallel to the direction of excitation, and some responses of walls orthogonal to the earthquake excitation.

MATHEMATICAL FORMULATION

The governing equation for the coupled fluid–structure system of the 3-D rectangular tank model given in Figure 1 is derived by minimizing a single functional defined for the entire system. The containing structure is assumed to be a linearly elastic isotropic medium with the fluid being inviscid and incompressible. The

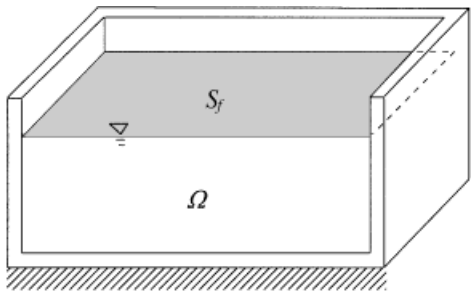

Figure 1. Cross-sectional view of a three-dimensional rectangular liquid storage tank model

irrotational motion of the ideal fluid is described by the velocity potential defined as

$$v_j = \frac{\partial \phi(\mathbf{x}, t)}{\partial x_j} \tag{1}$$

where $\mathbf{x} = (x_1, x_2, x_3)$ denotes the position vector; t the time variable; $\phi(\mathbf{x}, t)$ the velocity potential; and $\mathbf{v} = (v_1, v_2, v_3)$ the velocity vector of a fluid particle.

Following Luke[31] and Haroun,[32] a single Lagrange function (or, more appropriately, a functional) is defined for the motion of the fluid–structure system with the free fluid surface as follows:

$$\begin{aligned} &J(\mathbf{u}_o, \mathbf{u}_c, \dot{\mathbf{u}}_o, \dot{\mathbf{u}}_c, \phi, \xi, \dot{\xi}) \\ &= \int_{t_1}^{t_2} \left[T(\dot{\mathbf{u}}_o, \dot{\mathbf{u}}_c) - V(\mathbf{u}_o, \mathbf{u}_c) \right] \mathrm{d}t \\ &+ \int_{t_1}^{t_2} \left\{ -\frac{\rho_\ell}{2} \int_\Omega \nabla\phi \cdot \nabla\phi \, \mathrm{d}V + \rho_\ell \int_{S_f} \left(\dot{\xi}\phi - \frac{g\xi^2}{2} \right) \mathrm{d}s + \rho_\ell \int_{S_c} \dot{u}_{nc} \, \phi \, \mathrm{d}s \right\} \mathrm{d}t \end{aligned} \tag{2}$$

where T and V denote, respectively, the kinetic energy and the potential energy of the structure; $\mathbf{u}_c$ and $\mathbf{u}_o$ the degrees of freedom of the structure in contact with the fluid and those not in contact with the fluid, respectively; $\dot{\mathbf{u}}_c$ and $\dot{\mathbf{u}}_o$ are time derivatives of $\mathbf{u}_c$ and $\mathbf{u}_o$, respectively; ρ_ℓ means the fluid mass density; Ω, S_f and S_c denote the fluid domain, the free surface of the fluid region and the surface of the fluid region in contact with the structure, respectively; ξ and $\dot{\xi}$ indicate the vertical elevation of the free fluid surface from a reference level and its velocity, respectively; and $\dot{u}_{nc}$ means the normal velocity of the fluid particle in contact with the structure. In equation (2) the first integral denotes the component of the Lagrange function related to the motion of structure and the second integral the component associated with the fluid motion. The first term in the second integral of equation (2) can be converted into the surface integral by the identity,

$$\int_\Omega \nabla\phi \cdot \nabla\phi \, \mathrm{d}V = \int_{\partial\Omega} \phi \frac{\partial \phi}{\partial n} \mathrm{d}s \tag{3}$$

where $\partial\Omega = S_c + S_f$ and $\partial\phi/\partial n$ is the outward normal velocity.

By the finite element modelling of the motion of the structure, the kinetic energy T and the potential energy V of the structure can be expressed as

$$T = \frac{1}{2} \{\dot{\mathbf{u}}_o \; \dot{\mathbf{u}}_c\} [M] \begin{Bmatrix} \dot{\mathbf{u}}_o \\ \dot{\mathbf{u}}_c \end{Bmatrix} \tag{4a}$$

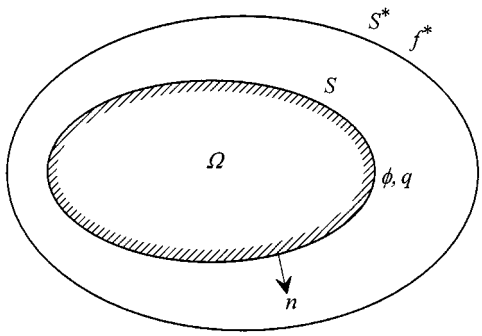

n : outward normal vector orthogonal to S
ϕ : potential at a point on S
q : outward flux at a point on S
f^*: distributed source on S^*

Figure 2. A finite fluid region Ω with its boundary S embedded on a large fluid region with the boundary S^*

and

$$V = \frac{1}{2}\{\mathbf{u}_o\ \mathbf{u}_c\}\,[K]\begin{Bmatrix}\mathbf{u}_o\\ \mathbf{u}_c\end{Bmatrix} \tag{4b}$$

where $[M]$ and $[K]$, respectively, are the symmetric mass and stiffness matrices of the structure model and can be written in the partitioned form such that

$$[M] = \begin{bmatrix} M_{oo} & M_{oc} \\ M_{co} & M_{cc} \end{bmatrix} \tag{5a}$$

and

$$[K] = \begin{bmatrix} K_{oo} & K_{oc} \\ K_{co} & K_{cc} \end{bmatrix} \tag{5b}$$

in which subscript c denotes the degrees of freedom of the structure in contact with the fluid and subscript o those degrees of freedom that are not in contact. In order to express the second integral of equation (2) with respect to the discrete degrees of freedom, an indirect boundary element method is employed. The fluid region, Ω under consideration with its boundary $\partial\Omega = S$ is assumed embedded on a larger fluid domain enclosed with the boundary, S^*, as shown in Figure 2. It is assumed further that the potential in Ω is defined by the sources, f^*, distributed over the auxiliary surface S^*. Then the potential, $\phi(\mathbf{x})$ and the outward normal flux, $q(\mathbf{x}) = \partial\phi/\partial n$ on the boundary S can be expressed by the expressions

$$\phi(\mathbf{x}) = \int_{S^*} G(\mathbf{x};\mathbf{y})\, f^*(\mathbf{y})\, \mathrm{d}s(\mathbf{y}) \tag{6}$$

and

$$q(\mathbf{x}) = \int_{S^*} H(\mathbf{x},\mathbf{n};\mathbf{z})\, f^*(\mathbf{z})\, \mathrm{d}s(\mathbf{z}) \tag{7}$$

where $\mathbf{x}$ is a point on the boundary S; $\mathbf{y}$ and $\mathbf{z}$ are points on the auxiliary boundary S^*; $G(\mathbf{x};\mathbf{y})$ is Green's function of the Laplace equation and denotes the potential at $\mathbf{x}$ due to a point source located at a point y;

$H(\mathbf{x}, \mathbf{n}; \mathbf{z})$ is the outward normal derivative of Green's function $G(\mathbf{x}; \mathbf{z})$ on the boundary S; and $\mathbf{n}$ denotes the outward unit normal vector.

If the strength of the distributed source is interpolated from the nodal values on the surface S^* in such a way that

$$f^*(\mathbf{y}) = \mathbf{N}^*(\mathbf{y})\, \mathbf{f}_e^*(\mathbf{y}) \tag{8}$$

where $\mathbf{N}^*$ denotes the row vector of shape functions used for the interpolation of source strength and $\mathbf{f}_e^*$ the nodal source strength vector defined on S^*, then equations (6) and (7) can be rewritten as

$$\phi(\mathbf{x}) = \left[\int_{S^*} G(\mathbf{x}; \mathbf{y}) \mathbf{N}^*(\mathbf{y})\, \mathrm{d}s^*(\mathbf{y}) \right] \mathbf{f}_e^* \tag{9}$$

and

$$q(\mathbf{x}) = \left[\int_{S^*} H(\mathbf{x}, \mathbf{n}; \mathbf{z}) \mathbf{N}^*(\mathbf{z})\, \mathrm{d}s^*(\mathbf{z}) \right] \mathbf{f}_e^* \tag{10}$$

Now, suppose that the boundary, S, of the fluid region Ω is discretized by the same interpolation formula used for the finite element modelling of the structure:

$$\xi(\mathbf{x}) = \mathbf{N}(\mathbf{x}) \xi_e \tag{11a}$$

and

$$\dot{u}_{nc}(\mathbf{x}) = \mathbf{N}(\mathbf{x}) \dot{\mathbf{u}}_{nce} \tag{11b}$$

where $\mathbf{N}$ is the row vector of shape functions for the interpolation of field variables on S, ξ_e the vector of nodal vertical elevations of the free fluid surface and $\dot{\mathbf{u}}_{nce}$ the vector of nodal values corresponding to $\dot{u}_{nc}$. Then introducing equations (3), (4), (9) and (10) into equation (2), the functional for the coupled fluid–structure system can be expressed in terms of the finite number of degrees of freedom:

$$\begin{aligned}
&J(\mathbf{u}_o, \mathbf{u}_c, \dot{\mathbf{u}}_o, \dot{\mathbf{u}}_c, \mathbf{f}_e, \xi_e, \dot{\xi}_e) \\
&= \int_{t_1}^{t_2} \left[\frac{1}{2} \{\dot{\mathbf{u}}_o\ \dot{\mathbf{u}}_c\} [M] \begin{Bmatrix} \dot{\mathbf{u}}_o \\ \dot{\mathbf{u}}_c \end{Bmatrix} - \frac{1}{2} \{\mathbf{u}_o\ \mathbf{u}_c\} [K] \begin{Bmatrix} \mathbf{u}_o \\ \mathbf{u}_c \end{Bmatrix} \right] \mathrm{d}t \\
&\quad - \int_{t_1}^{t_2} \frac{\rho_\ell}{2} \mathbf{f}_e^{*\mathrm{T}} \left[\int_S \mathrm{d}s(\mathbf{x}) \int_{S^*} \mathbf{N}^{*\mathrm{T}}(\mathbf{y}) G(\mathbf{x}; \mathbf{y})\, \mathrm{d}s^*(\mathbf{y}) \int_{S^*} H(\mathbf{x}, \mathbf{n}; \mathbf{z}) \mathbf{N}^*(\mathbf{z})\, \mathrm{d}s^*(\mathbf{z}) \right] \mathbf{f}_e^*\, \mathrm{d}t \\
&\quad + \int_{t_1}^{t_2} \rho_\ell \dot{\xi}_e^{\mathrm{T}} \left[\int_{S_f} \mathbf{N}^{\mathrm{T}}(\mathbf{x})\, \mathrm{d}s(\mathbf{x}) \int_{S^*} G(\mathbf{x}; \mathbf{y})\, \mathbf{N}^*(\mathbf{y})\, \mathrm{d}s^*(\mathbf{y}) \right] \mathbf{f}_e^*\, \mathrm{d}t \\
&\quad - \int_{t_1}^{t_2} \frac{g \rho_\ell}{2} \dot{\xi}_e^{\mathrm{T}} \left[\int_{S_f} \mathbf{N}^{\mathrm{T}}(\mathbf{x}) \mathbf{N}(\mathbf{x})\, \mathrm{d}s(\mathbf{x}) \right] \xi_e\, \mathrm{d}t \\
&\quad + \int_{t_1}^{t_2} \rho_\ell \dot{\mathbf{u}}_c^{\mathrm{T}}\, T_c^{\mathrm{T}} \left[\int_{S_c} \mathbf{N}^{\mathrm{T}}(\mathbf{x})\, \mathrm{d}s(\mathbf{x}) \int_{S^*} G(\mathbf{x}; \mathbf{y}) \mathbf{N}^*(\mathbf{y})\, \mathrm{d}s^*(\mathbf{y}) \right] \mathbf{f}_e^*\, \mathrm{d}t
\end{aligned} \tag{12}$$

where the superscript T denotes the transpose operation of matrices and matrix T_c is the transformation matrix which defines the relation between $\mathbf{u}_{nce}$ and $\mathbf{u}_c$ by

$$\mathbf{u}_{nce} = T_c \mathbf{u}_c \tag{13}$$

Applying Hamilton's principle to equation (12), the following set of equations is obtained:

$$[M]\begin{Bmatrix}\ddot{\mathbf{u}}_o\\ \ddot{\mathbf{u}}_c\end{Bmatrix}+[K]\begin{Bmatrix}\mathbf{u}_o\\ \mathbf{u}_c\end{Bmatrix}+[E]\{\mathbf{f}_e^*\}=\{0\} \tag{14a}$$

$$[A]\{\mathbf{f}_e^*\}-[B]^T\{\dot{\xi}_e\}-[E]^T\{\dot{\mathbf{u}}_c\}=\{0\} \tag{14b}$$

and

$$[B]\{\dot{\mathbf{f}}_e^*\}+[K_{ff}]\{\xi_e\}=\{0\} \tag{14c}$$

where

$$[A]=\frac{\rho_\ell}{2}\int_S \mathrm{d}s(\mathbf{x})\int_{S^*}\mathbf{N}^{*T}(\mathbf{y})G(\mathbf{x};\mathbf{y})\,\mathrm{d}s^*(\mathbf{y})\int_{S^*}H(\mathbf{x},\mathbf{n};\mathbf{z})\mathbf{N}^*(\mathbf{z})\,\mathrm{d}s^*(\mathbf{z}) \tag{15a}$$

$$[B]=\rho_\ell\int_{S_f}\mathbf{N}^T(\mathbf{x})\,\mathrm{d}s(\mathbf{x})\int_{S^*}G(\mathbf{x};\mathbf{y})\,\mathbf{N}^*(\mathbf{y})\,\mathrm{d}s^*(\mathbf{y}) \tag{15b}$$

$$[E]=\rho_\ell\,T_c^T\int_{S_c}\mathbf{N}^T(\mathbf{x})\,\mathrm{d}s(\mathbf{x})\int_{S^*}G(\mathbf{x};\mathbf{y})\,\mathbf{N}^*(\mathbf{y})\,\mathrm{d}s^*(\mathbf{y}) \tag{15c}$$

$$[K_{ff}]=\frac{g\rho_\ell}{2}\int_{S_f}\mathbf{N}^T(\mathbf{x})\,\mathbf{N}(\mathbf{x})\,\mathrm{d}s(\mathbf{x}) \tag{15d}$$

Equations (14a) and (14c) can be combined into the following single expression:

$$\begin{bmatrix}M_{oo}&M_{oc}&0\\ M_{co}&M_{cc}&0\\ 0&0&0\end{bmatrix}\begin{Bmatrix}\ddot{\mathbf{u}}_o\\ \ddot{\mathbf{u}}_c\\ \ddot{\xi}_e\end{Bmatrix}+\begin{bmatrix}K_{oo}&K_{oc}&0\\ K_{co}&K_{cc}&0\\ 0&0&K_{ff}\end{bmatrix}\begin{Bmatrix}\mathbf{u}_o\\ \mathbf{u}_c\\ \xi_e\end{Bmatrix}+\begin{bmatrix}0&0\\ 0&Q\end{bmatrix}\begin{Bmatrix}0\\ \dot{\mathbf{f}}_e^*\end{Bmatrix}=\{0\} \tag{16}$$

Assuming that the matrix A is nonsingular, $\mathbf{f}_e^*$ can be found from equation (14b) as

$$\dot{\mathbf{f}}_e^*=A^{-1}Q^T\begin{Bmatrix}\ddot{\mathbf{u}}_c\\ \ddot{\xi}_e\end{Bmatrix} \tag{17}$$

By substituting equation (17) into equation (16), the governing equation of the coupled fluid–structure system is obtained as follows:

$$\begin{bmatrix}M_{oo}&M_{oc}&0\\ M_{co}&M_{cc}+M_{cc}^A&M_{cf}^A\\ 0&M_{fc}^A&M_{ff}^A\end{bmatrix}\begin{Bmatrix}\ddot{\mathbf{u}}_o\\ \ddot{\mathbf{u}}_c\\ \ddot{\xi}_e\end{Bmatrix}+\begin{bmatrix}K_{oo}&K_{oc}&0\\ K_{co}&K_{cc}&0\\ 0&0&K_{ff}\end{bmatrix}\begin{Bmatrix}\mathbf{u}_o\\ \mathbf{u}_c\\ \xi_e\end{Bmatrix}=\{0\} \tag{18}$$

where M_{cc}^A, M_{cf}^A, M_{fc}^A and M_{ff}^A are partitioned matrices of the matrix, M^A which is the added fluid mass matrix given by

$$M^A=QA^{-1}Q^T \tag{19}$$

The added matrix M^A is symmetric because the self-adjointness of Laplace operator guarantees the symmetry of matrix A. It can be seen in equation (15d) that the matrix K_{ff} is also symmetric.

Since boundary conditions on S are prescribed in terms of potentials in many cases, it may be more convenient to take a variation of the functional in Equation (12) with respect to the nodal potential, ϕ_e, instead of the nodal source strength, $\mathbf{f}_e^*$. In this case $\mathbf{f}_e^*$ can be replaced by ϕ_e using the relation of equation (9) by applying the weighted residual method. The degrees of freedom in equation (18) are defined with respect to

the inertia reference frame. However, for seismic analysis it will be more appropriate to modify equation (18) into one in terms of quantities relative to the ground motion:

$$\begin{bmatrix} M_{oo} & M_{oc} & 0 \\ M_{co} & M_{cc}+M_{cc}^{A} & M_{cf}^{A} \\ 0 & M_{fc}^{A} & M_{ff}^{A} \end{bmatrix} \begin{Bmatrix} \ddot{\mathbf{u}}_o \\ \ddot{\mathbf{u}}_c \\ \ddot{\xi}_e \end{Bmatrix} + \begin{bmatrix} K_{oo} & K_{oc} & 0 \\ K_{co} & K_{cc} & 0 \\ 0 & 0 & K_{ff} \end{bmatrix} \begin{Bmatrix} \mathbf{u}_o \\ \mathbf{u}_c \\ \xi_e \end{Bmatrix} = - \begin{bmatrix} M_{oo} & M_{oc} & 0 \\ M_{co} & M_{cc}+M_{cc}^{A} & M_{cf}^{A} \\ 0 & M_{fc}^{A} & M_{ff}^{A} \end{bmatrix} [\mathbf{r}] \{\ddot{\mathbf{u}}_g\} \quad (20)$$

where $[\mathbf{r}]$ denotes the earthquake influence coefficient matrix, $\{\ddot{\mathbf{u}}_g\}$ the ground acceleration vector and all the degrees of freedom are interpreted as quantities relative to the ground motion.

The effects of damping can be included readily into the equations in the form of either generalized Rayleigh damping or modal damping. Because a double surface integration is required in the present formulation, the computation time is expected to be longer than the conventional direct BEM–FEM which requires only a single surface integration. The energy method used in the present derivation may look similar to those introduced in Reference 33. However, the functional defined in the present method has more direct physical meaning than those in other energy formulations.

COMPARISON WITH TEST RESULTS

The analysis results by the present method are compared with experimental results of shaking-table tests and the solutions obtained by the direct BEM–FEM[34] for the purpose of verification.

Shaking-table tests were performed with a 3-D rectangular tank model made of acrylic plates. The material properties are: the density, $\rho = 1200\ \text{kg/m}^3$; the Young's modulus, $E = 2{\cdot}9 \times 10^9\ \text{N/m}^2$; and the Poisson's ratio $\nu = 0{\cdot}35$. The model is designed according to the following geometric specifications defined in Figure 3: the height, $H = 0{\cdot}9$ m; the wall thickness, $t = 35$ mm; the length, $L = 2{\cdot}2$ m; and the width, $W = 1{\cdot}15$ m. The four corners of the model are strengthened with steel angles. To satisfy the rigid base assumption, a steel plate is attached to the bottom slab.

From the preliminary test performed with an empty tank model, the viscous damping ratio is found to be approximately 5%. The tank was then filled with water up to the depth of 0·7 m. Six pressure guages, twelve accelerometers and two water level guages were placed to measure the dynamic responses of the tanks. All the tests were conducted using the 6-DOF shaking table at the Korean Institute of Machinery and Metals.

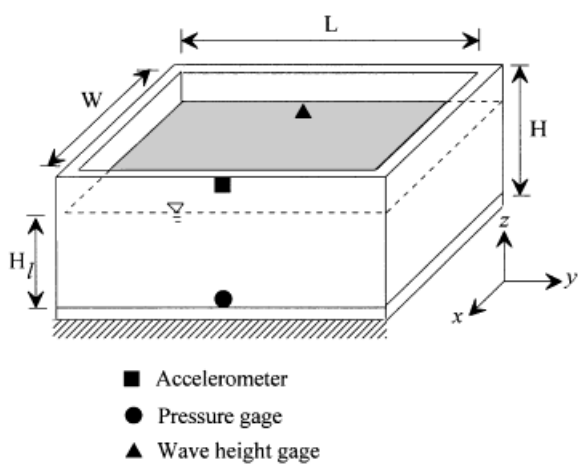

Figure 3. Three-dimensional rectangular liquid storage tank model

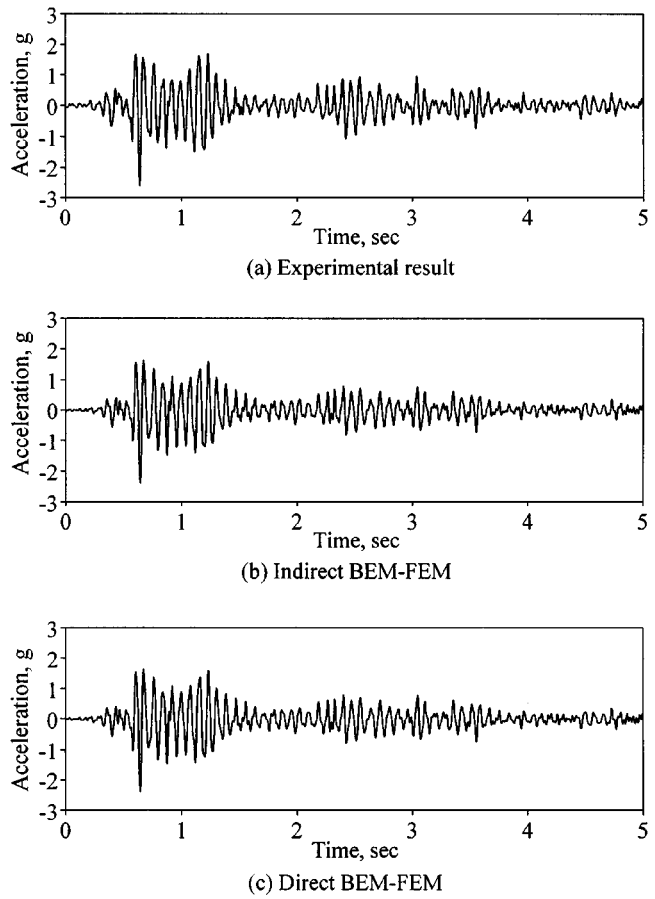

Figure 4. Comparison of acceleration time history measured at the top of the middle cross-section of the long side wall with analytical predictions

The N–S component of 1940 El Centro Earthquake records was time scaled with a factor of 4 and used as the input motion of shaking-table tests in the horizontal direction perpendicular to the long side walls. The measured peak table acceleration was $0{\cdot}22g$. Three response time histories measured at the locations shown in Figure 3 are presented: acceleration time history of the structure at the top of the middle cross-section of the long side wall in Figure 4; hydrodynamic pressure time history at the mid-point of the long side edge of the bottom slab surface in Figure 5; and fluid surface elevation at the middle cross-section of the long side wall in Figure 6.

The test structure was modelled by using 8-node plate finite elements[35] to compute the responses by the present BEM–FEM. The optimal distance from the auxilliary boundary to the real one in modelling the fluid region by the indirect BEM was found to be one-eighteenth (1/18) of the water depth, H_ℓ.

The agreement between the test results and the predicted ones by the present method appears to be very satisfactory in the time histories of the acceleration of the structure and the hydrodynamic pressure as shown in Figures 4 and 5. Comparison with the predicted results by the direct BEM–FEM is also in very good agreement. Although small discrepancy in the detailed shape of the sloshing response is observed, it is clearly shown in Figure 6 that the overall sloshing response is also in good agreement between the test results and the predicted ones. It should be noted that, while the solution of the sloshing response by the direct BEM–FEM depends on the size of elements used for modelling the fluid region, the solution by the indirect

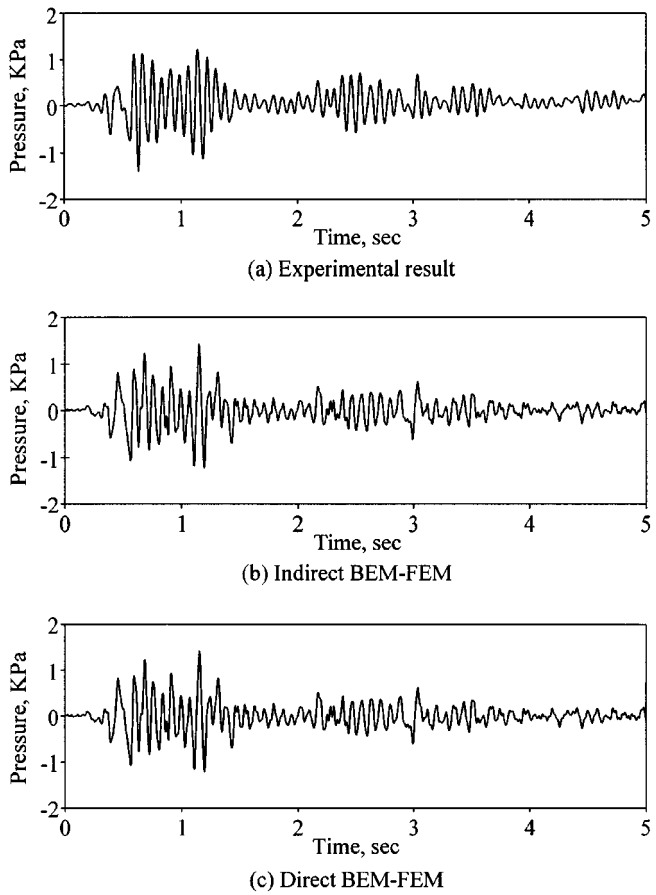

Figure 5. Comparison of hydrodynamic pressure measured at the intersection between the bottom slab and the middle cross-section of the long side wall with analytical predictions

BEM–FEM is more sensitive to the distance from the auxiliary boundary to the real one. As the distance increases, artificial high-frequency oscillations become more pronounced in the sloshing solution. Overall, the comparison confirms that the present method can be used with confidence for the dynamic analysis of rectangular tanks taking into account sloshing motion.

INVESTIGATION ON SEISMIC RESPONSES OF RECTANGULAR TANKS

The present method is now applied to investigate seismic response characteristics of 3-D rectangular fluid storage tanks. Since rectangular tanks are used most often for the wet-type storage of nuclear spent fuel assemblies, a typical dimension for those tanks is selected for the present investigation: the height of the wall, $H = 10$ m; the water depth, $H_\ell = 9$ m; the length of the short side wall, $W = 20$ m; and the length of the long side wall, $L = 50$ m, and typical material properties for the concrete tanks: the density, $\rho = 2400$ kg/m^3; the Young's modulus, $E = 2{\cdot}1 \times 10^{10}$ N/m^2; and the Poisson's ratio, $v = 0{\cdot}17$. Nuclear spent fuel storage tanks are usually designed with fairly thick side walls for the purpose of radioactive and thermal protection. In this study two different wall thickness are selected: $t = 1$ m for typical nuclear spent fuel storage tanks; and $t = 0{\cdot}5$ m for flexible rectangular liquid storage tanks. The tank is assumed to be fixed to the ground, and to have 3 per cent structural damping unless specified. The present study focuses on the effects of sloshing

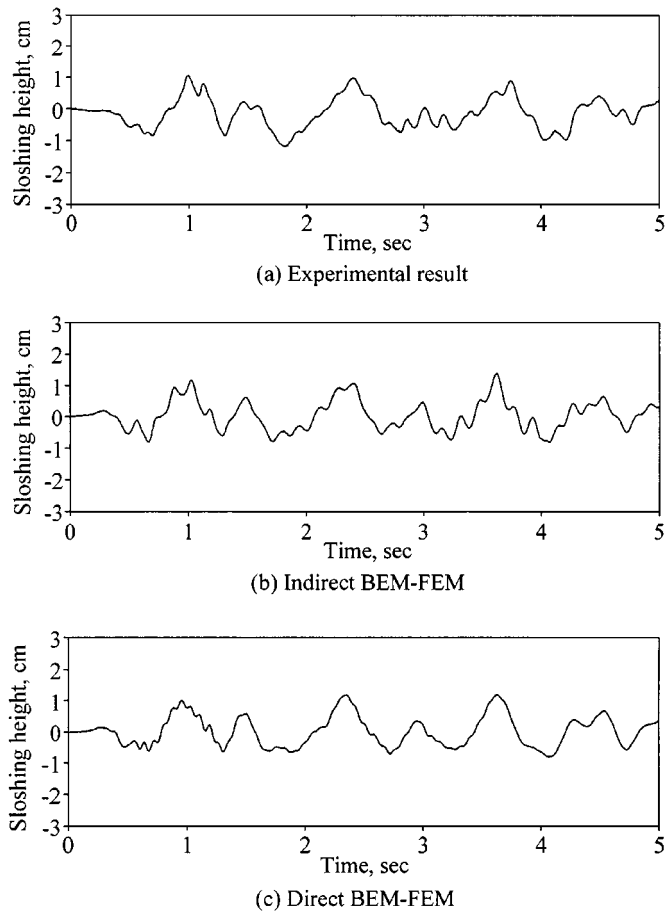

Figure 6. Comparison of liquid surface elevation at the middle cross-section of the long side wall with analytical predictions

motion and adjacent walls, which could not be dealt with in our previous detailed investigation of response characteristics for rectangular tanks by analytical methods.[15]

Sloshing response

To study the effects of wall flexibility on the sloshing motion and of surface waves on the dynamic responses, the analytical models with the two different wall thickness are analysed by the present method for horizontal ground excitation in the direction parallel to the short side walls. The N–S component of the 1940 El Centro Earthquake records is again used as an input motion.

Time histories of the sloshing motion at the middle cross-section of the long side wall are presented and compared with that of a corresponding rigid tank in Figure 7. The sloshing motion in the case of 1 m wall thickness is virtually identical to that of the rigid tank although there can be seen a small contribution from high-frequency sloshing motion due to the wall flexibility. The effect of wall flexibility becomes dominant when the wall thickness decreases as can be seen in the case of 0·5 m thickness. This was also confirmed by the numerical computation that natural frequencies of the interaction modes due to the wall flexibility became lower and closer to those of pure sloshing modes and thus the interaction modes participated more in the overall sloshing motion.

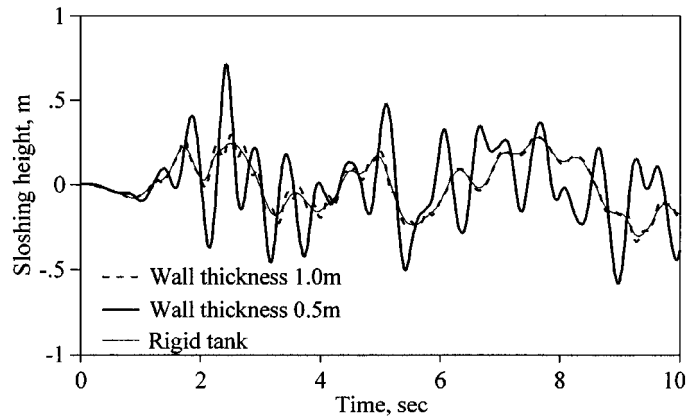

Figure 7. Time histories of liquid surface elevation at the middle cross-section of the long side wall by the indirect BEM–FEM

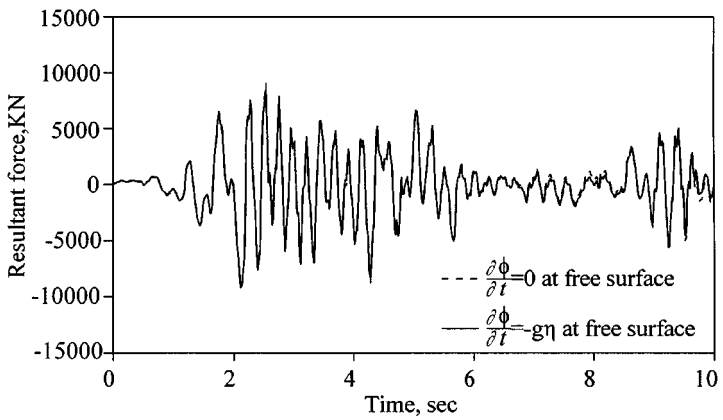

Figure 8. Time histories of resultant force acting on the long side wall for different liquid surface boundary conditions

To see the effects of the surface wave on the dynamic response of the structure, analyses are performed for two different liquid surface boundary conditions: (i) a pressure-free condition; and (ii) a linearized boundary condition. The time history of the resultant force acting on the middle cross-section of the long side wall of the tank model with 1 m thickness is presented in Figure 8. The difference between the two boundary cases is negligible, and the percentage of difference relative to the peak value is only 2·6 per cent. There is also little difference in the acceleration time histories at the top of the middle cross-section of the long side wall although they are not presented here. This fact can be further verified by identical pressure distribution over the long side wall for both cases when the resultant forces reach their peak values. Only the pressure distribution for the linearized free-surface boundary condition is presented in Figure 9, since that for the pressure-free boundary condition is indistinguishable. This fact is also found to be true for the case of a more flexible tank with 0·5 m wall thickness.

It may be thus concluded that the sloshing motion itself can be very much amplified due to the flexibility of the wall, but its effect on the dynamic response of the wall is negligible. It is worthy here to note that, even in the case of fairly thick walls, hydrodynamic pressure can be much amplified in the middle of the wall in rectangular tanks and shows the distribution of 2-D spatial variation over the surface of the wall as depicted in Figure 9.

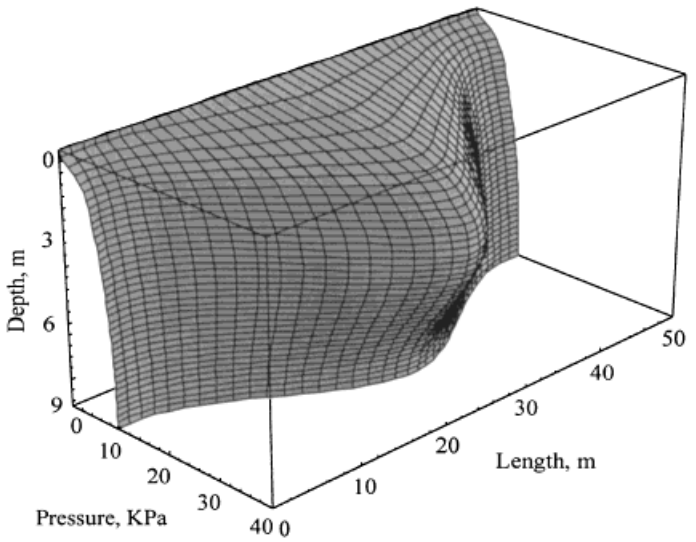

Figure 9. Pressure distribution on the long side wall at the moment when its resultant is maximum

Effect of rigidity of adjacent side walls

The dynamic response of 3-D rectangular tanks may be influenced by the constraint imposed by the walls parallel to the direction of ground motion. These walls are referred to as the adjacent side walls. The previous study[15] shows that the dynamic response of 3-D rectangular tanks can be strongly dependent on the assumed boundary conditions of the wall in analytical models. This implies that the rigidity of adjacent walls may play an important role in the dynamics of 3-D rectangular tanks and needs further investigation. To this end, 3-D rectangular tanks models with three different short side wall thickness, $t_S = 0{\cdot}5t$, $1{\cdot}0t$ and $2{\cdot}0t$ where t is the thickness of the long side wall under consideration, are analysed. As in the previous analysis, the N–S component of the 1940 El Centro Earthquake records is applied in the direction orthogonal to the long side walls.

The natural frequency of the first interaction mode and peak acceleration at the top of the middle cross-section of the long side wall are calculated for each model and listed in Table I. The frequency of the first interaction mode virtually does not change regardless of the thickness of walls and the relative rigidity of adjacent side walls. The change in the peak acceleration of the wall is not so small, but the change in the resulting pressure distribution along the height of the same cross-section is insignificant as can be seen in Figure 10. However, when the aspect ratio, L/H, of the long side wall is small, the frequency of the first interaction mode can change significantly as the rigidity of adjacent side walls varies. Table II shows the dynamic response of the tanks with respect to the adjacent side wall thickness when the aspect ratio, L/H, is 2·0. The change can result in a spectral acceleration which may exhibit a rapid fluctuation within the frequency range of interest, and the change in the distribution pattern of hydrodynamic pressure over the wall. Thus, the rigidity of adjacent side walls can play an important role as the restraint conditions of the long side walls when their aspect ratio is small, and accordingly affect the dynamic response of 3-D rectangular tanks. This effect becomes insignificant for the range of the aspect ratio greater than 4·0 (see also Figure 16 in Reference 15).

Response of walls orthogonal to earthquake excitation direction

Because of the geometry, the dynamic response of a 3-D rectangular tank may show some dependency on the direction of the applied earthquake excitation. Therefore, ground motions into two principal axes may

Table I. Dynamic responses of 3-D rectangular tanks with respect to the side wall thickness ($L/H = 5{\cdot}0$)

Long side wall thickness, t (m)	Adjacent side wall thickness, t_s	Frequency (Hz)	Acceleration (m/s^2)
1·0	0·5t	4·32	25·6
	1·0t	4·38	30·2
	2·0t	4·42	27·9
0·5	0·5t	1·88	35·0
	1·0t	1·88	36·8
	2·0t	1·88	41·3

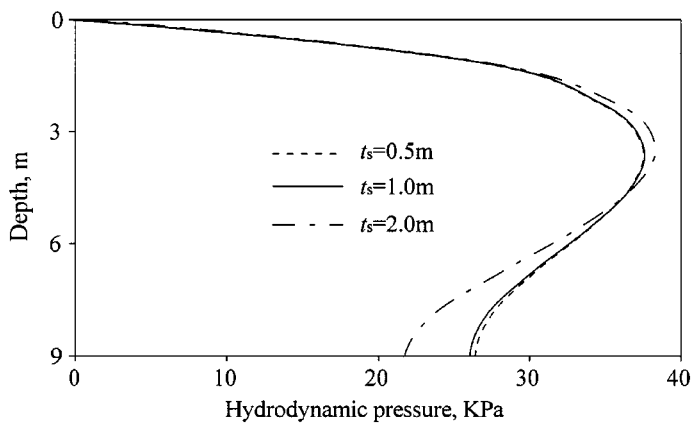

Figure 10. Pressure distributions along the height of the middle cross-section of the long side wall with respect to different adjacent wall thickness

Table II. Dynamic responses of 3-D rectangular tanks with respect to the side wall thickness ($L/H = 2{\cdot}0$)

Long side wall thickness, t (m)	Adjacent side wall thickness, t_s	Frequency [Hz]	Acceleration (m/s^2)
1·0	0·5t	6·09	13·6
	1·0t	6·93	16·9
	2·0t	7·71	21·6
0·5	0·5t	2·71	20·1
	1·0t	3·27	24·4
	2·0t	3·68	22·0

have to be considered in the seismic design of rectangular tanks. To this end, the dynamic response of the same tank model with the wall thickness of 1 m is analysed for horizontal ground excitation in the direction parallel to the long side walls. The E–W component of El Centro Earthquake records is used as an input ground acceleration.

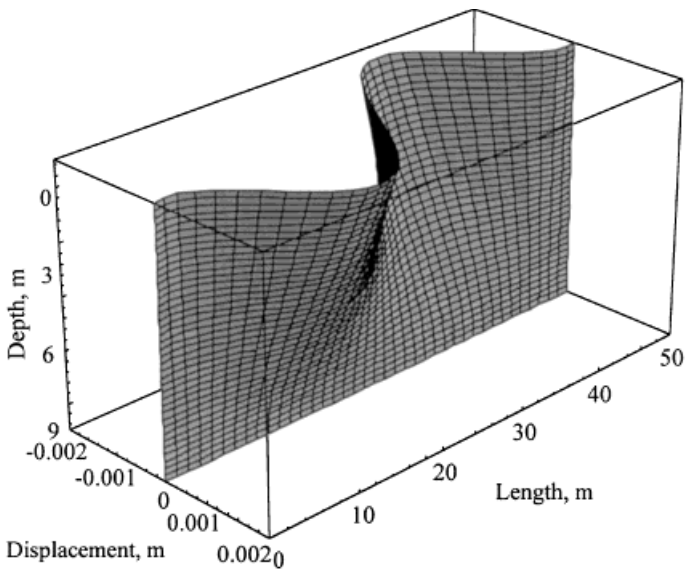

Figure 11. Deformed shape of the long side wall when the resultant force acting on the adjacent wall reaches its maximum

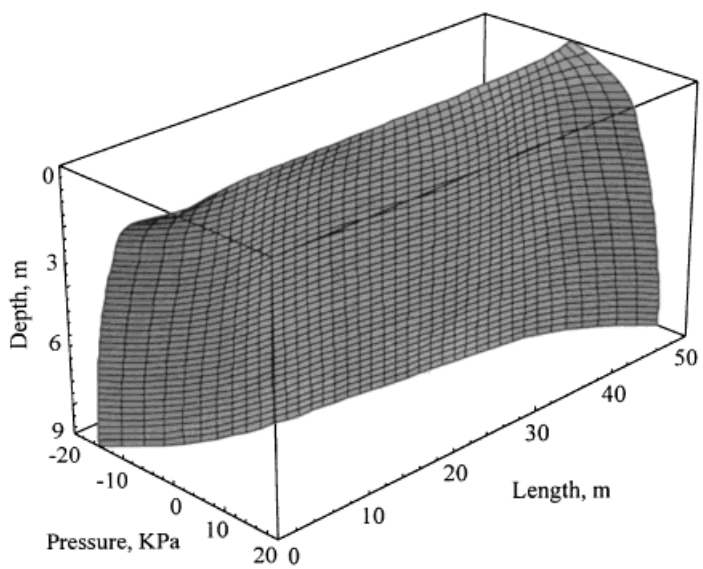

Figure 12. Pressure distribution on the long side wall when the resultant pressure acting on the adjacent wall reaches its maximum

The deformed shape of the long side wall and hydrodynamic pressure developed on the wall are presented in Figures 11 and 12, respectively, when the resultant force acting on the short side wall reaches its maximum. The deformed shape and hydrodynamic pressure distribution are anti-symmetric with respect to the plane of symmetry parallel to the short side wall. The magnitude of the pressure is generally constant and small over most of the long side wall except for a region near the edge. Similar analyses are repeated for tank models with different side wall thickness. While the pressure distribution on the short side wall depends on the

flexibility of the wall, the pressure pattern on the long side wall tends to remain insensitive to the change in the rigidity of adjacent walls. This fact may imply that the orthogonal effect in 3-D rectangular tanks is insignificant, but further investigation is needed for more complete conclusions.

CONCLUSIONS

A variationally coupled indirect BEM–FEM has been proposed for the dynamic analysis of rectangular liquid storage tanks including free-surface sloshing motion. The predictions by the proposed method are in very good agreement with the shaking-table test results of a small-scale 3-D rectangular tank model and with the solutions by the direct BEM–FEM. With the verified indirect BEM–FEM, characteristics of seismic response of a 3-D rectangular tank are studied in the time domain.

The effect of free-surface sloshing motion on the dynamic response of the structure is found to be insignificant, thus the sloshing response can be decoupled from the inertia response. However, the sloshing motion itself may be very much amplified due to the flexibility of the wall in rectangular tanks. When the sloshing motion is very important as in the case of nuclear spent fuel storage tanks, more elaborated analysis methods, such as the present method, should be used for an accurate estimation of the sloshing wave height. It is also confirmed in 3-D rectangular tanks that hydrodynamic pressure is much amplified in the middle of the wall and shows the distribution of 2-D spatial variation over the surface of the wall, even for the case of fairly thick walls as in nuclear spent fuel storage tanks.

The rigidity of adjacent side walls parallel to the direction of earthquake excitation can exert influence to some degree on the dynamic response of the walls perpendicular to the direction of earthquake excitation. When the aspect ratio, L/H, of the wall is small, interaction vibration modes can change significantly as the rigidity of adjacent side walls varies. The change can result in a spectral acceleration which may exhibit a rapid fluctuation within the frequency range of interest, and the change in the distribution pattern of the hydrodynamic pressure over the wall.

The orthogonal effect in 3-D rectangular tanks is not likely very pronounced according to the present investigation. The dynamic response of the long side wall appears to be insensitive to the change in the rigidity of the adjacent short side walls that are perpendicular to the direction of earthquake excitation. Since the present study is based on the analyses of particular 3-D rectangular tank models, a more general conclusions may not be appropriate at the present time. Nevertheless, the present analysis method and analysis results reported herein can help the understanding of the dynamic behaviour of 3-D rectangular tanks.

ACKNOWLEDGEMENTS

This research is partially supported by a grant from EESRI (Electrical Engineering and Science Research Institute) and KEPCO (Korea Electric Power Company). The writers wish to thank them for the support.

REFERENCES

1. F. G. Rammerstorfer, K. Sharf and F. D. Fisher, 'Storage tanks under earthquake loading', *Appl. Mech. Rev. ASME* **43**, 261–282 (1990).
2. D. D. Kana, 'Seismic response of flexible cylindrical liquid storage tanks', *Nucl. Engng. Des.* **52**, 185–199 (1979).
3. D. Fisher, 'Dynamic fluid effects in liquid-filled flexible cylindrical tanks', *Earthquake Engng. Struct. Dyn.* **7**, 587–601 (1979).
4. M. A. Haroun and G. W. Housner, 'Seismic design of liquid storage tanks', *J. Tech. Councils ASCE* **107**, 191–207 (1981a).
5. M. A. Haroun and G. W. Housner, 'Earthquake response of deformable liquid storage tanks', *J. Appl. Mech. ASME* **48**, 411–418 (1981b).
6. A. S. Veletsos, 'Seismic response and design of liquid storage tanks', *Guidelines for the Seismic Design of Oil and Gas Pipeline Systems*, Tech. Council on Lifeline Earthquake Engineering, ASCE, 255–370, New York, 1984.
7. A. S. Veletsos and Y. Tang, 'Soil–structure interaction effects for laterally excited liquid storage tanks', *Earthquake Eng. Struct. Dyn.* **19**, 473–496 (1990).
8. A. S. Veletsos and Y. Tang, 'Dynamics of vertically excited liquid storage tanks', *J. Struct. Eng. ASCE* **112**, 1228–1246 (1986).
9. A. S. Veletsos, Y. Tang and H. T. Tang, 'Dynamic response of flexibly supported liquid storage tanks', *J. Struct. Engng. ASCE* **118**, 264–283 (1992).

10. P. Malhotra and A. S. Veletsos, 'Uplifting response of unanchored liquid storage tanks', *J. Struct. Eng. ASCE* **120**, 3525–3547 (1994).
11. G. W. Housner, 'Dynamic pressure on accelerated fluid containers', *Bull. Seism. Soc. Amer.* **47**, 15–35 (1957).
12. G. W. Housner, 'The dynamic behavior of water tanks', *Bull. Seism. Soc. Amer.* **53**(2), 381–389 (1963).
13. M. A. Haroun, 'Stress analysis of rectangular walls under seismically induced hydrodynamic loads', *Bull. Seism. Soc. Amer.* **74**(3), 1031–1041 (1984).
14. J.-H. Park, H. M. Koh and J. Kim, 'Fluid–structure interaction analysis by coupled boundary element–finite element method in time domain', *Proc. of 7th Int. Conf. on Boundary Element Technology, BETECH/92*, Computational Mechanics Publications, Southampton, 89–92 (1990).
15. J. K. Kim, H. M. Koh and I. J. Kwahk, 'Dynamic response of rectangular flexible fluid containers', *J. Engng. Mech. ASCE* **122**, 807–817 (1996).
16. J. F. Hall and A. K. Chopra, 'Hydrodynamic effects in the dynamic response of concrete gravity dams', *Earthquake Engng. Struct. Dyn.* **10**, 333–345 (1982).
17. G. Fenves and A. K. Chopra, 'Earthquake analysis of concrete gravity dams including reservoir bottom absorption and dam–water–foundation rock interaction', *Earthquake Engng. Struct. Dyn.* **12**, 663–680 (1984).
18. V. Lotfi, J. M. Roesset and J. L. Tassoulas, 'A technique for the analysis of the response of dams to earthquakes', *Earthquake Engng. Struct. Dyn.* **15**, 463–490 (1987).
19. T. B. Bougacha and J. L. Tassoulas, 'Seismic response of gravity dams. II: effects of sediments', *J. Engng. mech.* **117**, 1839–1850 (1991).
20. J. W. Chavez and G. L. Fenves, 'Earthquake analysis of concrete gravity dams including base sliding', *Earthquake Engng. Struct. Dyn.* **24**, 673–686 (1995).
21. C. S. Porter and A. K. Chopra, 'Dynamic analysis of simple arch dams including hydrodynamic interaction', *Earthquake Engng. Struct. Dyn.* **9**, 573–597 (1981).
22. C. S. Porter and A. K. Chopra, 'Hydrodynamic effects in dynamic response of simple arch dams', *Earthquake Engng. Struct. Dyn.* **10**, 417–431 (1982).
23. J. F. Hall and A. K. Chopra, 'Dynamic analysis of arch dams including hydrodynamic effects', *J. Engng. Mech. ASCE* 109, 149–167 (1983).
24. C.-Y. Lin and J. L. Tassoulas, 'Three-dimensional dynamic analysis of dam–water–sediment system', *J. Eng. Mech.* **113**, 1945–1958 (1987).
25. M.-H. Wang and T.-K. Hung, 'Three-dimensional analysis of pressure on dams', *J. Engng. Mech. ASCE* **116**, 1290–1304 (1990).
26. C.-S. Tsai and G. C. Lee, 'Method for transient analysis of three dimensional dam–reservoir interactions', *J. Engng. Mech. ASCE* **116**, 2151–2172 (1990).
27. C. S. Tsai and G. C. Lee, 'Time-domain analysis of dam-reservoir system II: Substructure method', *J. Engng. Mech. ASCE* **117**, 2007–2026 (1990).
28. A. M. Jablonski and J. L. Humar, 'Three-dimensional boundary element reservoir model for seismic analysis of arch and gravity dams', *Earthquake Eng. Struct. Dyn.* **19**, 359–376 (1990).
29. D. H. Wolf and H. Bachman, 'Hydrodynamic-stiffness matrix based on boundary elements for time-domain dam–reservoir–soil analysis', *Earthquake Engng. Struct. Dyn.* **16**, 417–432 (1988).
30. J. L. Humar and A. M. Jablonski, 'Boundary element reservoir model for seismic analysis of gravity dams', *Earthquake Engng. Struct. Dyn.* **16**, 1129–1156 (1988).
31. J. C. Luke, 'A variational principle for a liquid with free surface', *J. Fluid Mech.* **27**, 395–397 (1967).
32. M. A. Haroun, 'Vibration studies and test of liquid storage tanks', *Earthquake Engng. Struct. Dyn.* **11**, 179–206 (1983).
33. P. K. Banerjee, *The Boundary Element Methods in Engineering*, 2nd edn, McGraw-Hill, New York, 1993.
34. H. M. Koh, J. Kim and J.-H. Park, 'Seismic analysis of rectangular liquid storage structure with submerged objects by a coupled finite element-boundary element method', *Proc. 13th Int. Conf. on Structural Mechanics in Reactor Technology*, Porto Alegre, Brazil, 1995, pp. 323–334.
35. R. D. Cook, D. S. Malkus and M. E. Plesha, *Concepts and Application of Finite Element Method*, Wiley, New York, 1989.

